ACS NANO
Cite This: ACS Nano 2018, 12, 5197−5206
www.acsnano.org

ARTICLE

Nuclear-Targeted Photothermal Therapy Prevents Cancer Recurrence with Near-Infrared Triggered Copper Sulfide Nanoparticles

Na Li, Qiaoqiao Sun, Zhengze Yu, Xiaonan Gao, Wei Pan, Xiuyan Wan, and Bo Tang*

College of Chemistry, Chemical Engineering and Materials Science, Key Laboratory of Molecular and Nano Probes, Ministry of Education, Collaborative Innovation Center of Functionalized Probes for Chemical Imaging in Universities of Shandong, Institute of Molecular and Nano Science, Shandong Normal University, Jinan 250014, P. R. China

Supporting Information

ABSTRACT: **Clinical cancer treatments nowadays still face the challenge of recurrence due to the residual cancer cells and minute lesions in surgeries or chemotherapies. To effectively address the problem, we introduce a strategy for constructing cancer cell nuclear-targeted copper sulfide nanoparticles (NPs) with a significant photothermal effect to completely kill residual cancer cells and prevent local cancer recurrence. The NPs could directly target the tumor cells and further enter the nucleus by the surface modification of RGD and TAT peptides. Under the irradiation of 980 nm near-infrared laser, the NPs rapidly increase the temperature of the nucleus, destroy the genetic substances, and ultimately lead to an exhaustive apoptosis of the cancer cells. *In vivo* experiments show that the designed NPs could effectively treat cancer and prevent the return of cancer with a single laser irradiation for 5 min. The photothermal therapy strategy with nuclear targeting for cancer therapy and anti-recurrence will provide more possibilities to develop efficient platforms for treating cancer.**

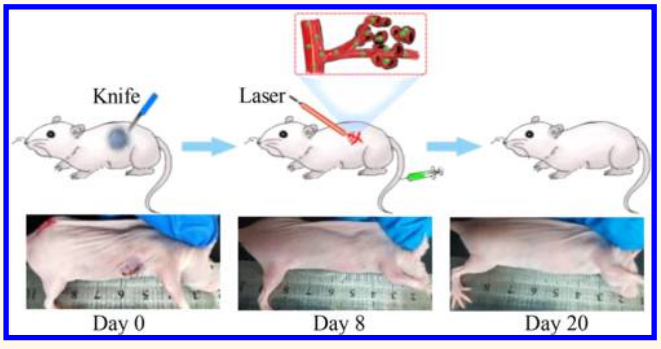

KEYWORDS: *nuclear-targeted, photothermal therapy, copper sulfide nanoparticles, cancer treatment, cancer recurrence*

Cancer, as one of the most complicated and intractable diseases that threatens human life and health,[1,2] has led to an increasing morbidity and mortality rate in the past few decades. Currently, the primary clinical cancer therapies comprise surgery, radiotherapy, and chemotherapy,[3,4] which possess therapeutic effects against most of the tumors. Despite continuous improvements of the techniques,[5−7] they are still limited to cancer recurrence caused by the residual microtumors,[8−11] which contain only a few cancer cells but enough to cause lethal recurrence. Such recurrence usually exhibits infinite proliferation and astonishing growth rate[12,13] due to the inexhaustive treatments. Hence, it is urgently needed to develop an efficient and specifically targeted method for completely massacring cancer cells and preventing recurrence in the future cancer therapies.

Photothermal therapy (PTT), as an emerging cancer treatment method,[14−16] is based on a light−heat conversion principle.[17−20] Under the irradiation of the external light source, nanoparticles (NPs) with high light−heat conversion efficiency could generate heat to kill tumor cells for cancer therapy.[14,21,22] Compared with other tumor treatments, PTT exhibits several advantages, such as precise light control on tumors, noninvasive penetration, and low toxicity to normal tissues.[23] Currently, most of the reported photothermal agents were located in the cytoplasm, which could reduce the therapeutic effect of PTT or cause unexpected damage to normal tissues. Considering that the nucleus is the most significant organelle in the cell and contains most of the intracellular genetic materials,[24−27] nuclear-targeted strategies could deliver the agents into the nucleus and greatly improve the therapeutic efficiency. Therefore, a nuclear-targeted photothermal agent is expected to directly destroy the genetic substances, efficiently kill tumor cells, and further prevent the recurrence.

In this study, a nuclear-targeted photothermal strategy based on copper sulfide nanoparticles (CuS NPs) was developed to

Received: September 27, 2017
Accepted: June 12, 2018
Published: June 12, 2018

DOI: 10.1021/acsnano.7b06870
ACS Nano 2018, 12, 5197−5206

achieve intranuclear PTT, which could thoroughly destroy residual cancer cells and effectively prevent local cancer recurrence. CuS NPs were considered as an optimal candidate for the core material due to some excellent properties, such as the outstanding near-infrared (NIR) optical absorption, the extraordinary molar extinction coefficient, the high photothermal conversion efficiency, and the metabolizability by humans.[28,29] Then, CuS NPs wrapped in oporous silica layers were prepared with an amino-functionalized surface. The as-prepared NPs were modified with TAT peptides as a nuclear targeting signal for efficient nuclear uptake by targeting the nuclear pore complex and entering the nuclei.[30] Then, RGD peptides were modified to bind to angiogenic endothelial cells, specifically, for the overexpression of integrin $\alpha_v\beta_3$, in contrast to its minimal expression in quiescent endothelial cells in most normal tissues. With an irradiation of a 980 nm laser, the heat generated from the NPs significantly increased the nucleus internal temperature, leading to the DNA damage and protein denaturation. Consequently, a complete cancer cell death and an irreversible cancer relapse will be realized using the nuclear-targeted PTT strategy (Scheme 1).

Scheme 1. Schematic Illustration of the Synthesis of the CuS@MSN-TAT-RGD NPs, and Photothermal Therapy in the Cell Nucleus with CuS NPs

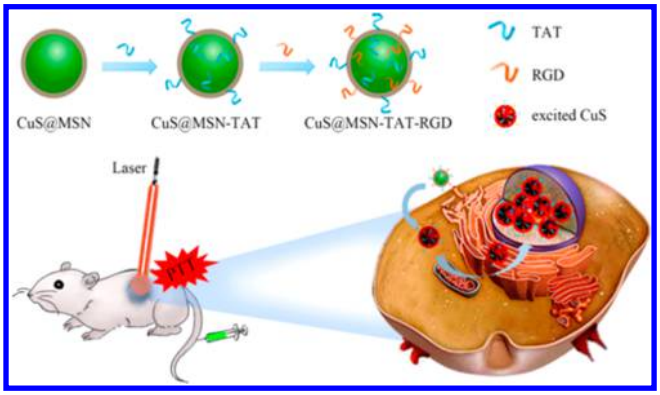

RESULTS AND DISCUSSION

Synthesis and Characterization of CuS@MSN. In order to modify target groups on the CuS NPs which possess an outstanding photothermal effect, mesoporous silica-coated CuS NPs (CuS@MSN) were rationally designed and synthesized. In the synthesis, the (3-aminopropyl)-triethoxysilane (APTES) silicon materials, which have been approved by the Food and Drug Administration (FDA), were applied for the encapsulation on the surface of CuS NPs.[31] According to the transmission electron microscope (TEM) images, the CuS NPs display a spherical shape and exhibit fine size dispersion with an average value of 10 nm (Figure 1A). In Figure 1B, the wrapped mesoporous silica NPs keep the spherical shape, and the average size rises to 40 nm, which makes them capable of transporting into the nucleus according to the previous literature.[32] In addition, zeta potential results confirmed the successful synthesis of the NPs, which are +32.1 ± 0.5 mV for CuS NPs due to the positively charged stabilizer CTAC, −23.9 ± 0.7 mV for CuS@MSN caused by the surface hydroxyl groups, and +7.2 ± 0.8 mV CuS@MSN-NH_2 for its amino modification (Figure S1). The optical properties of the NPs were investigated using UV−vis spectroscopy. The CuS NPs exhibit a significant characteristic absorption peak at 980 nm and stay after the surface MSN modification, indicating that the photothermal effect of CuS NPs cannot be affected by the silica wrapping (Figure 1C). The photothermal effect of CuS@MSN was studied under continuous laser irradiation (λ = 980 nm) at 1.5 W/cm^2 for 10 min. The temperature rapidly rose to 50 °C within 5 min and then remained stable at 53 °C. Simultaneously, an aqueous solution was applied as the control group, and its temperature rose from 25 to 37 °C (Figure 1D), which implies no damage to the tissue under laser irradiation. Therefore, it demonstrated that the temperature was high enough for cell apoptosis when irradiated with 1.5 W/cm^2 for 5 min, and there was no tissue damage in the absence of the NPs.[33] The result also matched with the photothermal images captured by the thermal camera (Figure 1E,F). Moreover, the photothermal conversion efficiency of CuS@MSN NPs was calculated to be 28.8% under the 980 nm (1.5 W cm^{-2}) laser irradiation (Figure S2). All results demonstrated that the CuS@MSN NPs were an ideal candidate as a nuclear-targeted photothermal agent due to their excellent photothermal effect and the suitable size.

CuS@MSN-TAT Synthesis and TAT Peptides Optimization. To evaluate the relationship between the nuclear targeting capability and the TAT concentration, co-localization imaging experiments in HeLa cells were performed. Hoechst 33342, a commercial nuclear dye, was employed to label the nucleus. FITC-labeled TAT peptides with were covalently bound to amine-functionalized CuS@MSN through an amido reaction with the carboxyl groups. The amount of TAT groups was optimized through the nuclear co-localization ability of the NPs. At first, a series of NPs (CuS@MSN-TAT-FITC) were prepared through adding different amounts of TAT peptides (0.4, 0.8, 1.6, 3.3, 6.6, and 8.0 μmol) in 10 mL of CuS@MSN solution. Then, HeLa cells were incubated with CuS@MSN-TAT-FITC for 12 h, and Hoechst 33342 was used to label the nuclei before the confocal imaging. The Pearson's correlation coefficient increased until the amount of TAT peptides reached 6.6 μmol (0.2661 μmol/mg CuS@MSN using a nanodrop method, Figure S3).

To further verify that TAT polypeptides could guide the NPs into the nucleus in the cells, CuS@MSN-RHB NPs and CuS@MSN-TAT-RHB NPs were also synthesized by anchoring rhodamine B (RHB) to the NPs surface. It clearly showed that the fluorescence of NPs was significantly enhanced after modification, demonstrating that RHB was successfully attached (Figure 1G). Then, The NPs' nucleus-entering ability was revealed on the HeLa cells using confocal laser scanning microscopy (CLSM) to study the co-localization. As shown in Figure 2B, most of NPs with TAT polypeptides are located in the nuclei, which display a purple color in the overlay channel. However, in the control group (Figure 2A), NPs without TAT polypeptides stayed in the cytoplasm. Similar results were obtained from Bio-TEM images and flow cytometry. CuS@MSN-TAT can indeed be transported into the nucleus, while CuS@MSN is located in the cytoplasm without TAT (Figure S4). Figure S5 also displayed the higher value of bright detail similarity, demonstrating the better degree of co-localization. Moreover, CuS@$SiO_{2(65)}$ NPs with an average size of 65 nm were also synthesized for comparison[29] (Figure S6). The CuS@$SiO_{2(65)}$-TAT rarely entered the nucleus and was mainly located in the cytoplasm (Figure S7). Those results indicated that the TAT polypeptides and the suitable size were the two key elements to ensure that the CuS NPs enter the nucleus.

DOI: 10.1021/acsnano.7b06870
ACS Nano 2018, 12, 5197−5206

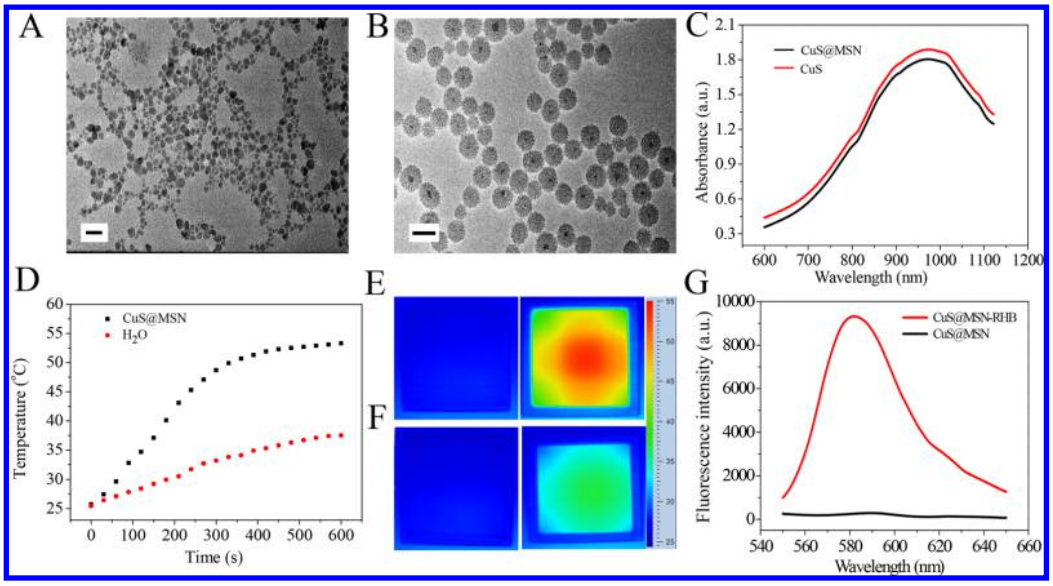

Figure 1. Characterization and photothermal effect of the nanoparticles. TEM images of (A) CuS-CTAC NPs and (B) CuS@MSN NPs; the scale bars are 50 nm. (C) UV−vis absorption spectra of CuS-CTAC NPs and CuS@MSN NPs. (D) The temperature change of CuS@MSN NPs in an aqueous solution as a function of 980 nm laser exposure time (laser power density: 1.5W/cm^2). (E) The photothermal images of CuS@MSN NPs in an aqueous solution before (left) and after (right) laser irradiation. (F) The photothermal images of water before (left) and after (right) laser irradiation. (G) The fluorescence emission spectra of CuS@MSN NPs and CuS@MSN-RHB NPs.

Therapeutic Effect of CuS@MSN-TAT *in Vitro*. For determining the optimum laser parameters in the cell and further investigating the therapeutic effect of photothermal NPs in the nucleus, 3-(4,5-dimethyl-thiazol-2-yl)-2,5-diphenyl-tetrazolium bromide (MTT) was employed.[34] HeLa cells treated with CuS@MSN-TAT were under a 980 nm laser irradiation with intensities of 0.8, 1.0, 1.5, and 2 W·cm^{-2} for 1−5 min, respectively. As shown in Figure 2C, under an irradiation of 0.8 W·cm^{-2}, the cell viability decreased gradually to 54% with longer irradiation time. By increasing the laser intensity to 1.0, 1.5, and 2.0 W·cm^{-2}, the cell viability dropped to 34%, 16.8%, and 16.2% with the same time period, respectively. Therefore, in clinical perspective, 1.5 W·cm^{-2} intensity and 5 min was chosen to avoid damage to normal cells but to kill cancer cells as the best endeavor. Moreover, CuS@MSN without TAT was also tested to show the pivotal role of TAT polypeptides as nuclear target groups. Figure 2D validated that only CuS@MSN-TAT performed a remarkably therapeutic effect as the cell viability reduced to 16.8%, while the viability of cells treated with CuS@MSN was much higher. To further prove that the pure NPs have no damage to cells, cells treated with NPs without light irradiation were tested. In Figure 2E, CuS@MSN and CuS@MSN-TAT without irradiation led to a cell viability of over 90%, but the laser group exhibited a significant decrease of the cell viability. Thus, the CuS@MSN-TAT with irradiation can effectively advance the therapeutic effect, whereas the NPs were substantially nontoxic and caused no damage to the normal cells without irradiation, even when they reached other tissues.

Intracellular DNA Damage Experiments. As the NPs entered into the nucleus of the cancer cells, it was assumed that the nucleus temperature significantly increased after the irradiation of the near-infrared laser, causing an irreversible damage to the DNA, protein, and other substances. Flow cytometry was carried out for statistical analysis of DNA immunofluorescence staining to determine the DNA damage. DNA damage, double strand breaks, will induce the phosphorylation of the H2A protein family proteins, H2AX. The phosphorylated protein, γ-H2AX, is responsible for the recruitment and locating the DNA repair mechanism, which is also an effective biomarker for double strand break detection. Flow cytometry analysis showed that the DNA immunofluorescence staining of the cancer cells treated with CuS@MSN-TAT displayed an enhanced green fluorescence, which verified the vital damage to the nucleus DNA (Figure 2F). Fluorescence intensity statistics also drew the same conclusion that CuS@MSN-TAT into the nucleus produced more severe DNA damage under laser irradiation (Figures 2G and S8).

Evaluation of the Therapeutic Effect of CuS@MSN-TAT *in Vivo*. The *in vivo* therapeutic effect of the designed NPs was also investigated in xenograft mouse models. HeLa cells were subcutaneously injected into the lower right forelimb of the mice, and the experiments were carried out when the tumors grew up to about 100 mm^3. The mice were then divided into five groups and intratumorally injected with different materials and a 980 nm laser irradiation (PBS only, PBS with irradiation, CuS@MSN with irradiation, and CuS@MSN-TAT and CuS@MSN-TAT with irradiation) to observe the body weight and tumor volume change (Figure 3A,B). After 14 days, the volume of the tumors in the mice treated with PBS and CuS@MSN-TAT without irradiation displayed a significant increase. However, the CuS@MSN-TAT and CuS@MSN with laser irradiation groups exhibited an inhibition of the tumor growth. Notably, the CuS@MSN-TAT with laser irradiation group owned a better efficiency, and the tumor almost disappeared. Moreover, the CuS@MSN-TAT showed nontoxicity since the changes in body weight were barely found (Figure 3C).

Targeting of CuS@MSN-TAT-RGD NPs to Cancer Cells. Even though *in vivo* intratumoral injection successfully inhibited the tumor growth, the actual clinical applications still process the difficulties of direct intratumoral injection. Therefore, applying NPs directly into targeted tumor cells and nucleus *via* intravenous injection will extraordinarily

DOI: 10.1021/acsnano.7b06870
ACS Nano 2018, 12, 5197−5206

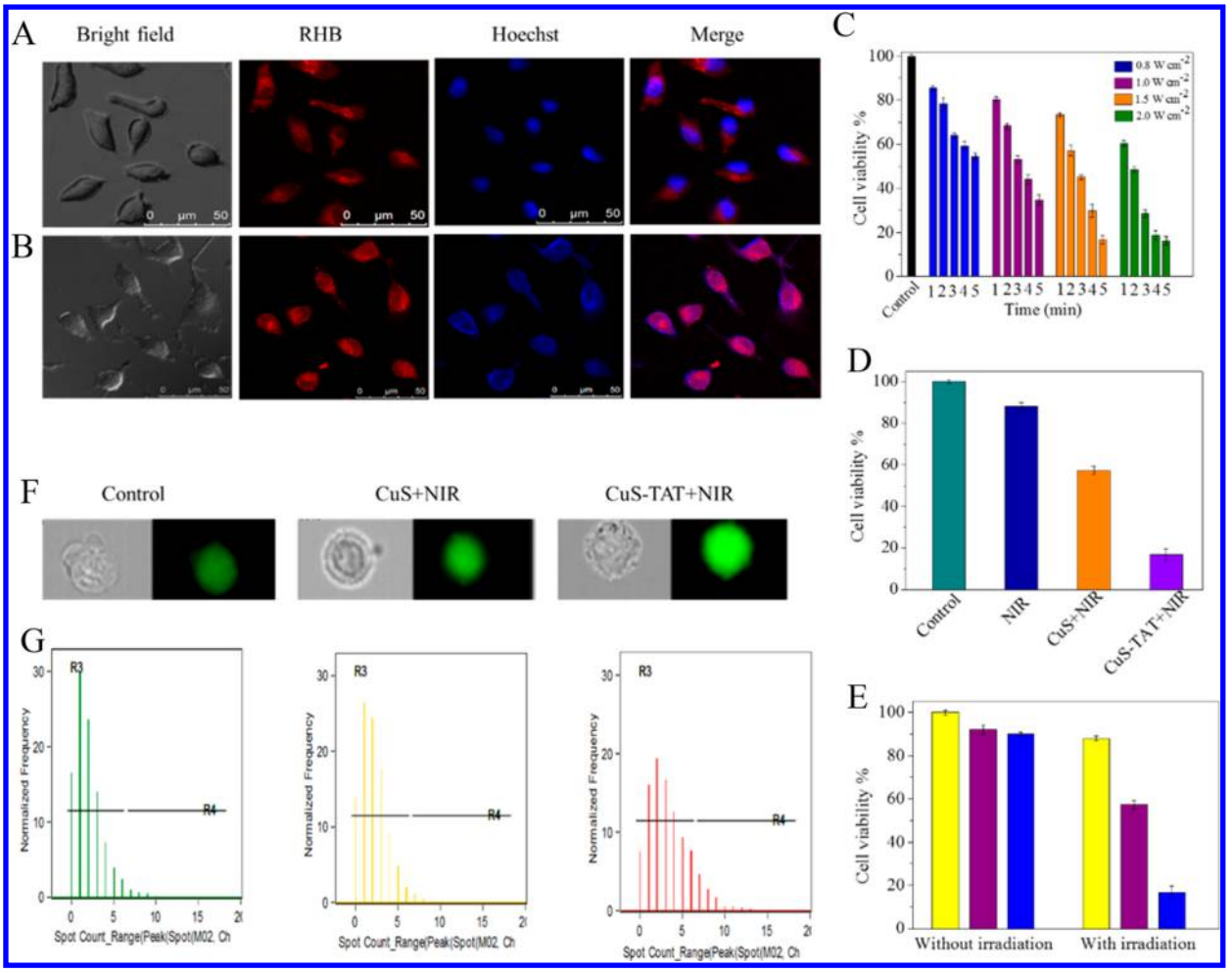

Figure 2. Co-localization images of the nuclear-targeted NPs and *in vitro* MTT assays, and flow cytometry imaging of DNA double strand breaks. Confocal images of HeLa cells after incubated with (A) CuS@MSN-RHB NPs and (B) CuS@MSN-TAT-RHB NPs. (C) Cell viability of HeLa cells treated with CuS@MSN-TAT (0.1 mg/mL) under various irradiation times (1, 2, 3, 4, and 5 min) and powers (0.8, 1.0 1.5, and 2.0 W/cm^2). (D) Cell viability after being subjected to different treatments. (E) Cell viability of HeLa cells with or without irradiation. The treatment of yellow color was PBS, the purple was CuS@MSN, and the blue was CuS@MSN-TAT. Intracellular verification of DNA double strand breaks in HeLa cells *via* γ-H2AX immunofluorescent staining using imaging flow cytometry. (F) Cell images after a different treatment (λ_{ex} = 488 nm, λ_{em} = 500−560 nm). (G) Flow cytometry data of the fluorescence intensity of cells under different treatments corresponding to cells. The treatment of the green color was control, the yellow was CuS+NIR, and the red was CuS+TAT+NIR.

enhance the applicability. In this regard, the RGD (arginine-glycine-aspartic) ring peptide was modified onto the surface of CuS@MSN-TAT *via* an amido bond for a cancer cell target purpose, and then the TAT polypeptide on the surface mediated the NPs into the nucleus. To maximize the targeting ability of the NPs, the amount of RGD groups was optimized through the cell uptake ability of the nanoparticles. RGD-linked CuS@MSN-TAT were prepared with various amounts of RGD groups (0, 0.15, 0.5, 1.5, 2.5, and 5.0 μmol) in 10 mL of CuS@MSN-TAT solution, respectively. After incubation for 2 h with Hela cells at the same concentration, the fluorescence intensity of cells was observed using CLSM. The quantified fluorescence intensity in each group revealed that the uptake of nanoparticles into the cells increased until the content of RGD reached 1.5 μmol, so 1.5 μmol was chosen in this study (Figure S9). The RGD loaded on the surface of the CuS nanoparticles was 0.0716 μmol/mg using the nanodrop method.

Next, the cancer cell targeting ability of the CuS@MSN-TAT-RGD was further assessed. From Figure 4A,B, the fluorescence intensity of red color in cervical cancer cells was higher than that in normal breast cells because the CuS@MSN-TAT-RGD could target cancer cells. RGD peptides of CuS@MSN-TAT-RGD NPs could specifically bind to integrin $\alpha v\beta 3$, which were overexpressed on the surface of cancer cells rather than normal cells. So, the uptake of CuS@MSN-TAT-RGD in HeLa cells was higher than that in normal breast cells under the same culture conditions.

***In Vivo* Tumor Imaging of CuS@MSN-TAT-RGD.** In order to investigate the transporting mechanism of the nanomaterial toward tumor tissues, RHB was attached to the CuS@MSN-TAT for *in vivo* imaging. As shown in Figure 4F, the red fluorescence accumulation at the tumor tissue gradually increased with the post-injection cumulative time and reached the maximum at 8 h, followed by a gradual decrease. Therefore, the photothermal treatment was carried out after an 8 h intravenous injection with CuS@MSN-TAT-RGD.

Since the electrons in the CuS NPs transit from the high energy level to the low energy level, the resulting rise in the cells' temperature of released energy will cause thermal expansion and a photoacoustic signal.[18] Hence, photoacoustic imaging was also applied to investigate the targeting ability of the NPs *in vivo*. First, the CuS NP-wrapped mesoporous silica

DOI: 10.1021/acsnano.7b06870
ACS Nano 2018, 12, 5197−5206

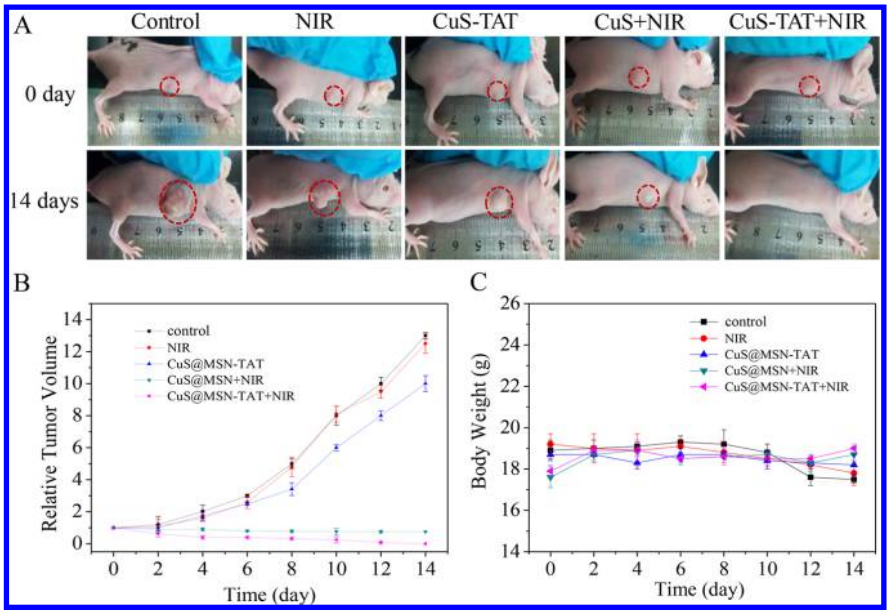

Figure 3. Therapeutic effect of NPs in mice *via* intratumoral injection. (A) Photographs of the mice before (0 day) and after (14 days) various indicated treatments: (i) PBS only (100 μL); (ii) PBS (100 μL) with laser irradiation for 5 min; (iii) CuS@MSN-TAT (100 μL, 1.0 mg/mL) only; (iv) CuS@MSN (100 μL, 1.0 mg/mL) with irradiation for 5 min; and (v) CuS@MSN-TAT (100 μL, 1.0 mg/mL) with irradiation for 5 min. The changes of tumor growth (B) and body weight (C) for mice with different treatments.

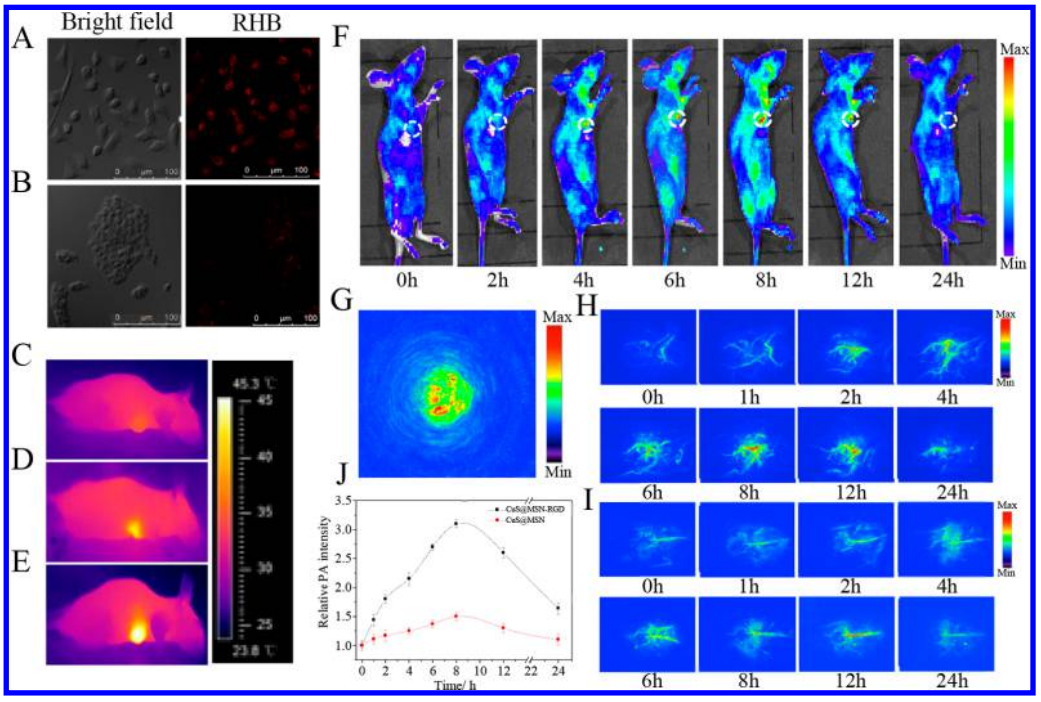

Figure 4. Confocal fluorescence imaging, *in vivo* photothermal imaging, *in vivo* fluorescence imaging, and photoacoustic imaging. Confocal images of HeLa cells (A) and normal breast cells (B). The cells were incubated with CuS@MSN-TAT-RGD (0.1 mg/mL). The photothermal images of the mice subcutaneous transplantation tumor were recorded by an infrared imager. The mice were treated with PBS (C), CuS@MSN (D), and CuS@MSN-TAT-RGD (E) *via* intravenous injection. For photothermal imaging, at 8 h post-injection, mice were irradiated under 980 nm laser for 5 min. (F) The fluorescent living imaging of nude mice treated with CuS@MSN-RHB-TAT-RGD. (G) Photoacoustic imaging of CuS@MSN in water solution. Photoacoustic imaging of a tumor which was cultured subcutaneously into the flanks of nude mice. The mice were treated with CuS@MSN-TAT-RGD (H) and CuS@MSN (I) *via* intravenous injection. (J) The relative intensity of the PA signal in H (black) and I (red) at the corresponding times.

layers displayed an obvious photoacoustic signal, indicating that the synthesized NPs can be used for photoacoustic imaging (Figure 4G). Typically, CuS@MSN and CuS@MSN-TAT-RGD were intravenously injected into two groups of mice, respectively. In Figure 4H,J, few blood vessels can be seen at the tumor tissues at the beginning, the photoacoustic signal gradually increased over time. With the continuous accumulation of the NPs until 8 h, the signal intensity reached the maximum and then weakened afterward. Compared with the control group, RGD-modified NPs clearly exhibited an

DOI: 10.1021/acsnano.7b06870
ACS Nano 2018, 12, 5197−5206

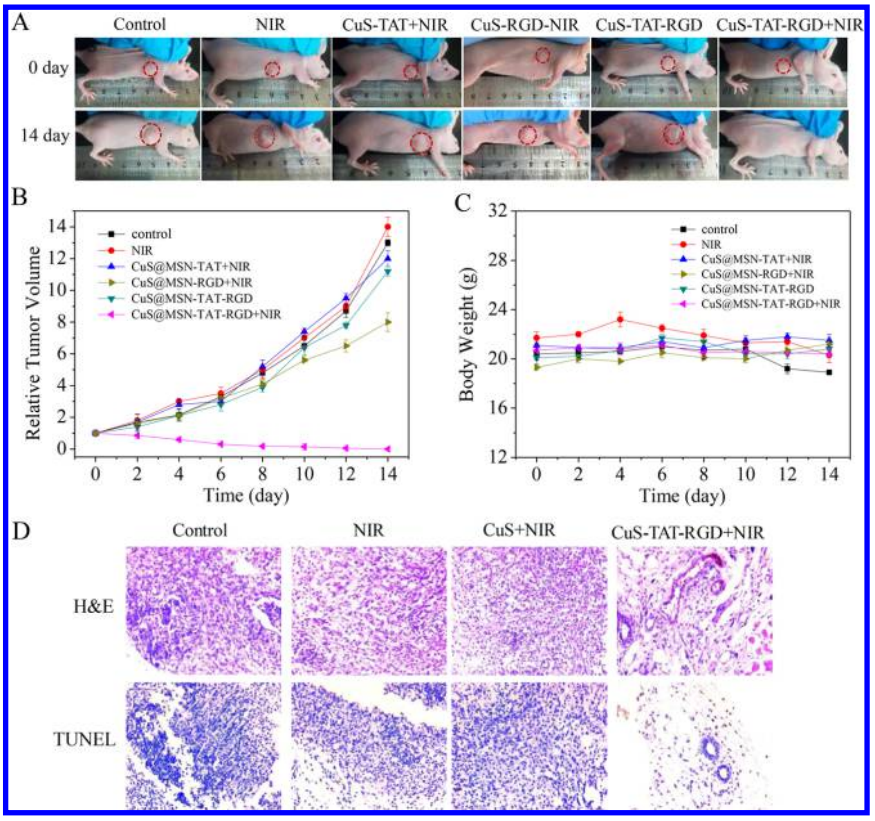

Figure 5. Therapeutic effect of NPs in mice *via* intravenous injection, H&E staining, and TUNEL staining. (A) Photographs of the mice before (0 day) and after (14 days) being subjected to different treatments: (i) PBS only (100 μL); (ii) PBS (100 μL) with laser irradiation for 5 min; (iii) CuS@MSN-TAT (100 μL, 1.0 mg/mL) with irradiation for 5 min; (iv) CuS@MSN-TAT-RGD (100 μL, 1.0 mg/mL) only; and (v) CuS@MSN-TAT-RGD (100 μL, 1.0 mg/mL) with irradiation for 5 min. The changes of tumor growth (B) and body weight (C) of mice in different groups. They were measured at a 2 day interval for 14 days. (D) H&E staining and TUNEL staining of the HeLa tumor. The tumors were treated differently: the control group, irradiation only, CuS@MSN with irradiation for 5 min, and CuS@MSN-TAT with irradiation for 5 min. The power density of the irradiation was 1.5 W·cm^{-2}.

enhanced signal, which proved the better targeting effect (Figure 4I). Subsequently, an infrared imager was used to picture the mice for thermal images, and CuS@MSN-TAT-RGD-treated mice demonstrated a higher temperature than the other groups in the tumor area, which further confirmed the thermal therapeutic effect of the NPs (Figure 4C,D,E).

Evaluation of the Therapeutic Effect of CuS@MSN-TAT-RGD *in Vivo*. For the next step, PBS, CuS@MSN-TAT, CuS@MSN-RGD, and CuS@MSN-TAT-RGD were intravenously injected into six groups of mice, respectively. Then, the mice were irradiated with a 980 nm laser for 5 min, after a circulation of 8 h. The tumor growth and mouse weight changes were recorded every other day within 14 days. The tumors of the CuS@MSN-TAT-RGD treatment group disappeared completely, whereas the tumor volumes in the control group expanded about 14 times (Figure 5A,B). In addition, three other groups of mice treated with PBS with irradiation, CuS@MSN-TAT with irradiation, and CuS@MSN-TAT-RGD without irradiation were studied for comparison, all of which showed about a 10 time increase of the tumor volume, and the group of CuS@MSN-TAT with irradiation showed about an 8 time increase. The biodistribution of CuS@MSN-RGD and CuS@MSN-TAT NPs at 8 h post-intravenous injection was then evaluated. The targeting effect of CuS@MSN-RGD was calculated to be 8.9% ID/g, while that of CuS@MSN-TAT was only 2.1% ID/g, which indicated that RGD modification could achieve the cancer cell target purpose. In addition, all of those groups showed no obvious body weight changes (Figure 5C). These suggested that the synthesized NPs could be effectively applied in treating tumors cells and possessed an excellent therapeutic effect when intravenously injected into the body.

Tissue Sections. Then we used the histological method to study the anticancer conditions of NPs. The tumor tissue was first stained with H&E and TUNEL, respectively. Tissue treated with CuS@MSN-TAT-RGD displayed a large area of broken pieces and shrinkage, while tumors in other groups were still normal (Figure 5D). Similarly, the TUNEL stained groups exhibited the similar results, demonstrating the outstanding outcome of CuS@MSN-TAT-RGD in tumor treatment. Other organs of the mice, including heart, liver, spleen, lung, and kidney, did not appear clear of cell apoptosis, proving that the NPs themselves were nontoxic to the normal tissues (Figure S10).

Inhibition Tumor Recurrence by CuS@MSN-TAT-RGD. In order to study the tumor recurrence prevention effect of the CuS@MSN-TAT-RGD, the resection was first used on a tumor-burdened mice tumor, and then different NPs were intravenously injected into the mice. As shown in Figure 6B, the group of mice with the intravenous injection of CuS@MSN-TAT-RGD and followed by irradiation at 8 h post-injection did not have any tumor recurrence, even measured up to 20 days. However, all of the control groups, including PBS alone, or the injection of CuS@MSN, CuS@MSN-TAT, and

DOI: 10.1021/acsnano.7b06870
ACS Nano 2018, 12, 5197−5206

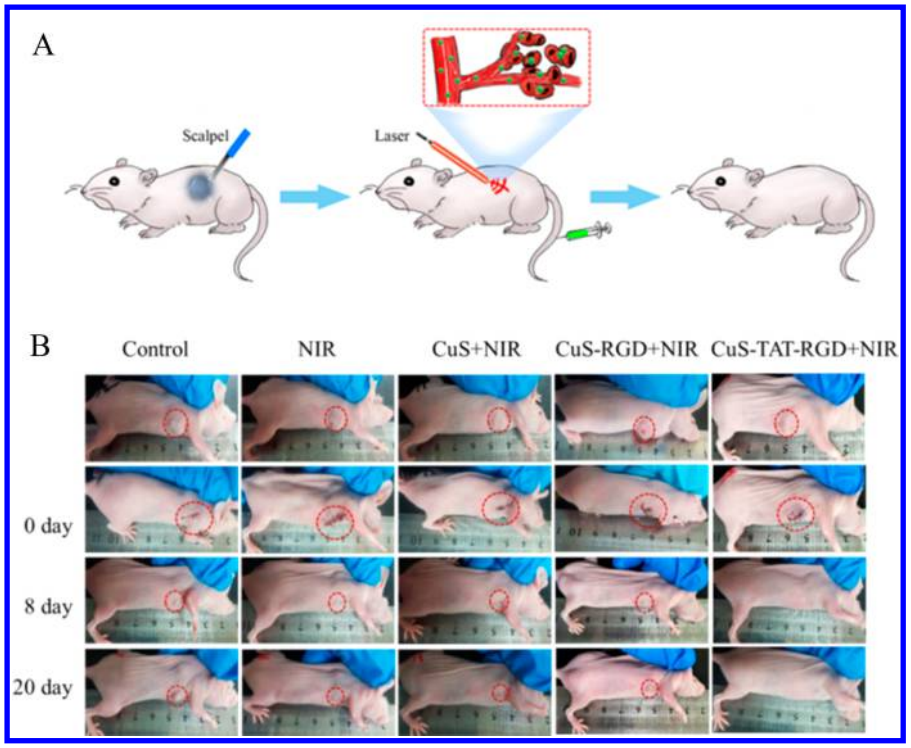

Figure 6. ***In vivo*** **tumor recurrence after surgical resection. (A)** ***In vivo*** **targeting tumor recurrence treatment process diagram. (B) Photographs of nude mice tumor recurrence with different processing after tumor resection. The NPs (100 μL, 1.0 mg/mL) were intravenously injected into the mice** ***via*** **tail vein at day 0. Then mice were recorded for 20 days at a 2 day interval.**

CuS@MSN-RGD groups had certain different degrees of recurrence. In particular, the CuS@MSN-RGD group displayed a significant recurrence, demonstrating that the nuclear-targeted photothermal effect was more effective in preventing recurrence. The weight profile measured at a 2 day interval for 20 days indicated that all of the groups of mice had no significant changes in body weight. (Figure S11).

CONCLUSION

In summary, we have prepared nuclear-targeted CuS NPs for near-infrared triggered PTT to treat cancer and avoid cancer recurrence. The NPs exhibited an outstanding targeting effect toward the cancer cells and further nucleus due to the surface decoration of RGD peptides. Confocal fluorescence imaging demonstrated that the NPs could effectively localize into the nucleus in living cells. The cell activity experiments showed that the mortality of targeted NPs is 84% with a single irradiation of 980 nm near-infrared laser for 5 min, while the mortality of nontargeted NPs is 42%. Notably, *in vivo* experiments indicated that the xenografted tumor was completely removed after 14 days with only one treatment, and there was no recurrence of the cancer, which further confirmed the excellent therapeutic effect of the designed NPs. Compared with the existing PTT, the cancer cell nuclear-targeted NPs could ultimately destroy nuclear function and eliminate cancer cells, thereby effectively preventing the recurrence of cancer. We anticipate that this nuclear targeting method for PTT can offer more opportunities in designing efficient platforms for cancer treatment.

MATERIALS AND METHODS

Materials and Reagents. Copper(II) chloride ($CuCl_2$), sodium sulfide ($Na_2S{\cdot}9H_2O$) tetraethyl orthosilicate (TEOS), triethanolamine (TEA), and cetyltrimethylammonium chloride (CTAC) were purchased from China National Pharmaceutical (Shanghai, China). RHB isothiocyanate and MTT were purchased from Sigma. APTES, *N*-hydroxysuccinimide (NHS), and 1-ethyl-3-(3-(dimethylamino)-propyl) carbodiimide hydrochloride (EDC) were purchased from Alfa Aesar (Tianjin, China). RGD and TAT (TAT: YGRKKRRQRRR) peptides were purchased from VIPbiochem (Wuhan, China). Fluorescein isothiocyanate (FITC)-TAT peptides (TAT: YGRKKRRQRRR) were synthesized by GenScript (Jiangsu, China). All chemicals were used as received without further purification. The human HeLa cell line was obtained from KeyGEN Biotechnology (Nanjing, China). Sartorius ultrapure water (18.2 MΩ cm) was used throughout the experiments.

Synthesis of CuS Nanoparticles. The whole process for the synthesis of CuS NPs was in aqueous solution. First, 20 mL of $CuCl_2$ water solution (0.85 mg/mL), 80 μL of CTAC (50 mg/150 μL), and 80 mL of water were mixed under stirring at room temperature. After 30 min, 50 μL of Na_2S (60.54 mg/250 μL) was added to the mixture and stirred for another 5 min. Then, the reaction solution was heated to 90 °C and continued to stir for 15 min until the dark-brown solution turned to dark green. Finally, the solution was transferred to ice-cold water. The CTAC-coated CuS NPs were obtained and stored at 4 °C.

Synthesis of CuS@MSN and CuS@MSN-NH_2. CTAC (0.0625 g) and TEA (12 mg) were dissolved in 10 mL of prepared CuS water solution, and the mixture was stirred for 1 h. Then, 100 μL of TEOS was slowly added to the mixture, and the resulting mixture was transferred to the oil bath under stirring at 85−90 °C. After 1 h, the mixture was centrifuged to collect the CuS@MSN. Water was used for washing. A 1 wt % solution of NaCl in methanol was repeated to remove the excess CTAC. Then, APTES was added to 10 mL of CuS@MSN to obtain CuS@MSN-NH_2. The final products were washed with ethanol three times to remove free APTES.

Synthesis of TAT Peptide-Modified CuS@MSN. TAT peptides were covalently bound to amine-functionalized CuS@MSN by an EDC/NHS coupling reaction with the carboxyl groups. First, in order to activate the carboxylic terminal group of the TAT peptide, 6.6 μmol TAT and 6.6 and 16.5 μmol NHS were dissolved in phosphate

DOI: 10.1021/acsnano.7b06870
ACS Nano 2018, 12, 5197−5206

buffered saline (PBS) solution (pH 7.4). Then, the mixture was placed at room temperature under magnetic stirring for 15 min. Subsequently, 10 mL of PBS solution of CuS@MSN was injected into the above solution and mixed for 24 h. Finally, the CuS@MSN was repeatedly washed with distilled water several times to remove the redundant TAT, EDC, and NHS. The CuS@MSN-TAT peptides were dispersed in water and stored at 4 °C.

Conjugation of Rhodamine B Isothiocyanate on CuS@MSN-NH_2 NPs. CuS@MSN-RHB was prepared successively by coupling the isothiocyanate groups of the RHB with amino groups on the surface. In this work, the amino group-functionalized CuS@MSN NPs were centrifuged and redispersed in 10 mL of MES buffer (10 mM, pH 6.0). Next, RHB isothiocyanate was added to the mixture and gently stirred for 12 h in the dark at room temperature. Finally, the particles were repeatedly washed with distilled water several times to make sure the redundant RHB was removed entirely.

Synthesis of RGD Peptide-Modified CuS@MSN. For the purpose of the conjugation of the RGD peptides, bifunctional *N*-hydroxysulfo-succinimide-polyoxyethylene-maleimide (NHS-PEG_{2000}-MAL) was used as a linker. Particularly, 10 mg of NHS-PEG_{2000}-MAL was grafted to CuS@MSN by conjugating NHS onto an amine-functionalized CuS@MSN. Then, by the addition reaction between the thiol groups in cysteine and the maleimide of NHS-PEG_{2000}-MAL, the RGD peptides (0, 0.15, 0.5, 1.5, 2.5, and 5.0 μmol) were added to 10 mL of CuS@MSN-TAT solution, respectively. In detail, the CuS@MSN-NH_2 was first reacted with NHS-PEG_{2000}-MAL in PBS with magnetic stirring for 12 h at room temperature, and the CuS@MSNs-PEG-MAL was obtained. Finally, CuS@MSNs-PEG-MAL continued to stir for 24 h at room temperature to react with the thiol groups of c(RGDyC).

TAT Peptide Concentration Optimization. A series of nanoparticles with different amounts of TAT (CuS@MSN-TAT-FITC) (100 μg/mL) in DMEM culture medium were respectively added to the confocal dish. HeLa cells were incubated with CuS@MSN-TAT-FITC for 4 h. After that, the original solution was replaced by fresh DMEM culture medium. After another 8 h, the residual NPs were removed by washing with PBS buffer, and the nuclei were labeled with Hoechst 33342 before the imaging experiment. A 405 nm excitation for Hoechst 33342 (emission = 430−480 nm) and a 488 nm excitation for FITC (emission = 500−550 nm) were employed.

Intracellular Localization Profile of NPs in HeLa Cells by CLSM. HeLa cells were first cultured in a confocal dish for 24 h. Then, CuS@MSN-RHB-TAT and CuS@MSN-RHB (100 μg/mL) in DMEM culture medium were respectively added to the confocal dish. The cells were incubated for 4 h. After that, the original solution was replaced by the fresh DMEM medium. After another 8 h, the residual NPs were removed by PBS buffer. Then, the Hoechst 33342 were added to stain the nuclei for 15 min. Lastly, the products were observed by CLSM, and confocal images were acquired for Hoechst 33342 (λ_{ex} = 405 nm, λ_{em} = 430−480 nm) and RHB (λ_{ex} = 543 nm, λ_{em} = 560−660 nm).

Co-localization Analysis of NPs in HeLa Cells by Imaging Flow Cytometer. HeLa cells (2×10^6) were incubated with CuS@MSN-RHB and CuS@MSN-TAT-FITC (100 μg/mL) for 4 h. After that, the original solution was replaced by fresh DMEM medium. After another 8 h, the residual NPs were removed by PBS buffer. Then, all groups of the cells were trypsinized and centrifuged (1000 rpm, 3 min), and the nuclei were labeled with Hoechst 33342. The PBS buffer was then used to wash the cells three times. Cell images were observed using the multispectral imaging flow cytometer (Amnis Corporation) with FITC (λ_{ex} = 488 nm, λ_{em} = 500−560 nm), RHB (λ_{ex} = 543 nm, λ_{em} = 560−660 nm), and Hoechst 33342 (λ_{ex} = 405 nm, λ_{em} = 430−480 nm). IDEAS image analysis (Amnis) software was used to analyze the images.

RGD Concentration Optimization. The amount of RGD groups was optimized through the cell uptake ability of the nanoparticles. RGD-linked CuS@MSN-TAT were prepared with various amounts of RGD groups (0, 0.15, 0.5, 1.5, 2.5, and 5.0 μmol) in 10 mL of CuS@MSN-TAT solution. After incubation for 2 h with Hela cells at the same concentration, the fluorescence intensity of the cells was measured using CLSM.

***In Vitro* Therapeutic Effects.** (1) HeLa cells were incubated in 96-well microliter plates for 24 h. CuS@MSN-TAT (0.1 mg/mL) in DMEM culture medium was added to the cells. After 12 h, the residual NPs were removed by PBS buffer. Then, the cells were treated with irradiation of disparate laser powers (0.8, 1, 1.5, and 2 W·cm^{-2}, respectively) and disparate irradiation times (1, 2, 3, 4, and 5 min, respectively). The control group was without any treatment. Then, the cells were incubated for another 24 h, and the MTT solution was added to cultivate for 4 h. Next, after removing the MTT solution, 150 μL of DMSO was injected to each well. (2) HeLa cells were incubated in 96-well microliter plates for 24 h. CuS@MSN and CuS@MSN-TAT (0.1 mg/mL) in DMEM culture medium were added to the cells. After 12 h, the residual NPs were removed by PBS buffer. Then, the cells were treated with irradiation (980 nm, 1.5 W·cm^{-2}, 5 min). The control group was without any treatment. Finally, the next procedures were according to that mentioned above. (3) HeLa cells were incubated in 96-well microliter plates for 24 h. CuS@MSN and CuS@MSN-TAT (0.1 mg/mL) in DMEM culture medium were added to the cells. After 12 h, the cells were washed with PBS buffer to remove the NPs that were not ingested into the cells. Then, the cells were treated with irradiation (980 nm, 1.5 W·cm^{-2}, 5 min). The cells were divided into two groups by with or without irradiation. The control group was without any treatment. Finally, the next procedures were according to that mentioned above. The absorbance was measured at 490 nm with a microplate reader.

***In Vitro* DNA Damage Study.** The H2A.X Phosphorylation Assay Kit was used to detect the DNA damage. Briefly, 2×10^6 HeLa cells were incubated with CuS@MSN and CuS@MSN-TAT (0.1 mg/mL) for 12 h, respectively, and irradiated with a 980 nm laser for 5 min. Then, all of the groups of cells were trypsinized and centrifuged (1000 rpm, 3 min). In order to fix the cells, 1X fixation solution was added at a cell density of 2×10^6 per mL and then incubated in ice for 20 min. After that, PBS buffer was used to wash the cells to remove the fixative. The cells pellets were then slowly resuspend in 1X permeabilization solution at a density of 2×10^6 cells per mL (50 μL per 1×10^5 cells). Subsequently, both the negative control FITC-conjugated normal mouse IgG and FITC-conjugated antiphospho-histone H2A.X (Ser139) (3.5 μL/1×10^5 cells) were added, and the cells were placed on ice for 20 min. One milliliter of 1X wash solution was added to remove the excess FITC-labeled antibody. Cell images were observed using the multispectral imaging flow cytometer (Amnis Corporation) with a 488 nm excitation for FITC (emission = 500−560 nm). The images were analyzed using IDEAS image analysis software (Amnis).

***In Vivo* PA Imaging, Fluorescence Imaging, and Photothermal Imaging.** Two groups of female Balb/c mice bearing HeLa tumors were treated with CuS@MSN or CuS@MSN-TAT-RGD (or CuS@MSN-RHB-TAT-RGD) *via* intravenous injection, respectively. Before taking images, the mice were narcotized by chloral hydrate, and PA images were acquired under a 980 nm irradiation at different post-injection times (0, 2, 4, 6, 8, 12, and 24 h). For fluorescence imaging, the experimental procedures were basically the same as the PA imaging. For photothermal imaging at 8 h post-injection, the mice were irradiated under a 980 nm laser for 5 min. Then, the photothermal images were obtained by an infrared thermal imaging instrument.

Therapeutic Efficacy of NPs *via* Injection. (1) The tumor-bearing mice were respectively intratumorally injected with PBS only, laser only, CuS@MSN-TAT only, CuS@MSN combined with laser irradiation, and CuS@MSN-TAT combined with laser irradiation. After 8 h, the tumor region was irradiated with a 980 nm laser (1.5 W·cm^{-2}) for 5 min. (2) The tumor-bearing mice were divided into six groups. The treatments were respectively PBS only, laser only, CuS@MSN-TAT only, CuS@MSN combined with laser irradiation, CuS@MSN-RGD combined with laser irradiation, and CuS@MSN-TAT-RGD combined with laser irradiation. PBS (100 μL) and 100 μL of 1.0 mg/mL of CuS@MSN, CuS@MSN-RGD, or CuS@MSN-TAT-RGD in PBS were intravenously injected into the mice *via* tail vein.

DOI: 10.1021/acsnano.7b06870
ACS Nano 2018, 12, 5197−5206

After 8 h, the tumor region was irradiated with a 980 nm laser (1.5 W·cm^{-2}) for 5 min. The mice body weights and the tumor size were observed every other day for 14 days.

***In Vivo* Antitumor Efficacy of Relapse.** About 10 days after HeLa tumor cells were transplanted into the flanks of mice (the tumor reaches ~300 mm^3), the tumors were cut out, leaving little remnant tissue behind. Then, the nude mice were weighed and randomly divided into 5 groups. The treatments were respectively PBS only, laser only, CuS@MSN-RGD combined with laser irradiation, CuS@MSN combined with laser irradiation, and CuS@MSN-TAT-RGD combined with laser irradiation. PBS (100 μL) and 100 μL of 1.0 mg/mL of CuS@MSN, CuS@MSN-RGD, or CuS@MSN-TAT-RGD in PBS were intravenously injected into the mice *via* tail vein. After 8 h, the tumor region was irradiated with a 980 nm laser (1.5 W·cm^{-2}) for 5 min. The body weights of the mice were observed every other day.

ASSOCIATED CONTENT

Supporting Information

The Supporting Information is available free of charge on the ACS Publications website at DOI: 10.1021/acsnano.7b06870.

Instruments, cell culture, animal tumor xenograft models, calculation of the photothermal conversion efficiency, and supporting figures (PDF)

AUTHOR INFORMATION

Corresponding Author

*E-mail: tangb@sdnu.edu.cn.

ORCID

Bo Tang: 0000-0002-8712-7025

Notes

The authors declare no competing financial interest.

ACKNOWLEDGMENTS

This work was supported by the National Natural Science Foundation of China (21390411, 21535004, 91753111, 21775094, and 21505087) and Natural Science Foundation for Distinguished Young Scholars of Shandong Province (JQ201503).

REFERENCES

(1) Siegel, R.; Naishadham, D.; Jemal, A. Cancer Statistics, 2013. *Ca-Cancer J. Clin.* **2013**, *63*, 11−30.

(2) Tian, J.; Ding, L.; Ju, H.; Yang, Y.; Li, X.; Shen, Z.; Zhu, Z.; Yu, J.-S.; Yang, C. J. A Multifunctional Nanomicelle for Real-Time Targeted Imaging and Precise Near-Infrared Cancer Therapy. *Angew. Chem., Int. Ed.* **2014**, *53* (36), 9544−9549.

(3) Pan, L.; Liu, J.; He, Q.; Wang, L.; Shi, J. Overcoming Multidrug Resistance of Cancer Cells by Direct Intranuclear Drug Delivery Using TAT-Conjugated Mesoporous Silica Nanoparticles. *Biomaterials* **2013**, *34*, 2719−2730.

(4) Zhou, H.; Qian, W.; Uckun, F. M.; Wang, L.; Wang, Y. A.; Chen, H.; Kooby, D.; Yu, Q.; Lipowska, M.; Staley, C. A.; Mao, H.; Yang, L. IGF1 Receptor Targeted Theranostic Nanoparticles for Targeted and Image-Guided Therapy of Pancreatic Cancer. *ACS Nano* **2015**, *9*, 7976−7991.

(5) Chen, Q.; Xu, L.; Liang, C.; Wang, C.; Peng, R.; Liu, Z. Photothermal Therapy with Immune-Adjuvant Nanoparticles Together with Checkpoint Blockade for Effective Cancer Immunotherapy. *Nat. Commun.* **2016**, *7*, 13193−13206.

(6) He, C.; Duan, X.; Guo, N.; Chan, C.; Poon, C.; Weichselbaum, R. R.; Lin, W. Core-shell Nanoscale Coordination Polymers Combine Chemotherapy and Photodynamic Therapy to Potentiate Checkpoint Blockade Cancer Immunotherapy. *Nat. Commun.* **2016**, *7*, 12499−12511.

(7) Muthana, M.; Kennerley, A. J.; Hughes, R.; Fagnano, E.; Richardson, J.; Paul, M.; Murdoch, C.; Wright, F.; Payne, C.; Lythgoe, M. F.; Farrow, N.; Dobson, J.; Conner, J.; Wild, J. M.; Lewis, C. Directing Cell Therapy to Anatomic Target Sites *In Vivo* with Magnetic Resonance Targeting. *Nat. Commun.* **2015**, *6*, 8009−8020.

(8) Conde, J.; Oliva, N.; Zhang, Y.; Artzi, N. Local Triple-Combination Therapy Results in Tumour Regression and Prevents Recurrence in a Colon Cancer Model. *Nat. Mater.* **2016**, *15*, 1128−1138.

(9) Duriez, E.; Masselon, C. D.; Mesmin, C.; Court, M.; Demeure, K.; Allory, Y.; Malats, N.; Matondo, M.; Radvanyi, F.; Garin, J.; Domon, B. Large-Scale SRM Screen of Urothelial Bladder Cancer Candidate Biomarkers in Urine. *Proteome Res.* **2017**, *16*, 1617−1631.

(10) Huang, X.; Tang, S.; Mu, X.; Dai, Y.; Chen, G.; Zhou, Z.; Ruan, F.; Yang, Z.; Zheng, N. Freestanding Palladium Nanosheets with Plasmonic and Catalytic Properties. *Nat. Nanotechnol.* **2011**, *6*, 28−32.

(11) Lukianova-Hleb, E. Y.; Kim, Y. S.; Belatsarkouski, I.; Gillenwater, A. M.; O'Neill, B. E.; Lapotko, D. O. Intraoperative Diagnostics and Elimination of Residual Microtumours with Plasmonic Nanobubbles. *Nat. Nanotechnol.* **2016**, *11*, 525−532.

(12) Chaffer, C. L.; Weinberg, R. A. A Perspective on Cancer Cell Metastasis. *Science* **2011**, *331*, 1559−1564.

(13) Jain, M.; Nilsson, R.; Sharma, S.; Madhusudhan, N.; Kitami, T.; Souza, A. L.; Kafri, R.; Kirschner, M. W.; Clish, C. B.; Mootha, V. K. Metabolite Profiling Identifies a Key Role for Glycine in Rapid Cancer Cell Proliferation. *Science* **2012**, *336*, 1040−1044.

(14) Cheng, L.; Yang, K.; Chen, Q.; Liu, Z. Organic Stealth Nanoparticles for Highly Effective *In Vivo* Near-Infrared Photothermal Therapy of Cancer. *ACS Nano* **2012**, *6*, 5605−5613.

(15) Guo, L.; Yan, D. D.; Yang, D.; Li, Y.; Wang, X.; Zalewski, O.; Yan, B.; Lu, W. Combinatorial Photothermal and Immuno Cancer Therapy Using Chitosan-Coated Hollow Copper Sulfide Nanoparticles. *ACS Nano* **2014**, *8*, 5670−5681.

(16) Liu, H.; Chen, D.; Li, L.; Liu, T.; Tan, L.; Wu, X.; Tang, F. Multifunctional Gold Nanoshells on Silica Nanorattles: A Platform for the Combination of Photothermal Therapy and Chemotherapy with Low Systemic Toxicity. *Angew. Chem., Int. Ed.* **2011**, *50*, 891−895.

(17) Meng, Z.; Wei, F.; Wang, R.; Xia, M.; Chen, Z.; Wang, H.; Zhu, M. NIR-Laser-Switched *In Vivo* Smart Nanocapsules for Synergic Photothermal and Chemotherapy of Tumors. *Adv. Mater.* **2016**, *28*, 245−253.

(18) Yu, Z.; Wang, M.; Pan, W.; Wang, H.; Li, N.; Tang, B. Tumor Microenvironment-Triggered Fabrication of Gold Nanomachines for Tumor-Specific Photoacoustic Imaging and Photothermal Therapy. *Chem. Sci.* **2017**, *8*, 4896−4903.

(19) Wang, Y.; Wang, K.; Zhao, J.; Liu, X.; Bu, J.; Yan, X.; Huang, R. Multifunctional Mesoporous Silica-Coated Graphene Nanosheet Used for Chemo-Photothermal Synergistic Targeted Therapy of Glioma. *J. Am. Chem. Soc.* **2013**, *135*, 4799−4804.

(20) Xiao, Q.; Zheng, X.; Bu, W.; Ge, W.; Zhang, S.; Chen, F.; Xing, H.; Ren, Q.; Fan, W.; Zhao, K.; Hua, Y. Q.; Shi, J. L. A Core/Satellite Multifunctional Nanotheranostic for *In Vivo* Imaging and Tumor Eradication by Radiation/Photothermal Synergistic Therapy. *J. Am. Chem. Soc.* **2013**, *135*, 13041−13048.

(21) Zou, Q.; Abbas, M.; Zhao, L.; Li, S.; Shen, G.; Yan, X. Biological Photothermal Nanodots Based on Self-Assembly of Peptide-Porphyrin Conjugates for Antitumor Therapy. *J. Am. Chem. Soc.* **2017**, *139*, 1921−1927.

(22) Zhao, X.; Yang, C.-X.; Chen, L.-G.; Yan, X.-P. Dual-Stimuli Responsive and Reversibly Activatable Theranostic Nanoprobe for Precision Tumor-Targeting and Fluorescence-Guided Photothermal Therapy. *Nat. Commun.* **2017**, *8*, 14998−15007.

(23) Zhu, X.; Feng, W.; Chang, J.; Tan, Y. W.; Li, J.; Chen, M.; Sun, Y.; Li, F. Temperature-Feedback Upconversion Nanocomposite for Accurate Photothermal Therapy at Facile Temperature. *Nat. Commun.* **2016**, *7*, 10437−10447.

(24) Huo, S.; Jin, S.; Ma, X.; Xue, X.; Yang, K.; Kumar, A.; Wang, P. C.; Zhang, J.; Hu, Z.; Liang, X.-J. Ultrasmall Gold Nanoparticles as

Carriers for Nucleus-Based Gene Therapy Due to Size-Dependent Nuclear Entry. *ACS Nano* **2014**, *8*, 5852−5862.
(25) Pan, L.; He, Q.; Liu, J.; Chen, Y.; Ma, M.; Zhang, L.; Shi, J. Nuclear-Targeted Drug Delivery of TAT Peptide-Conjugated Monodisperse Mesoporous Silica Nanoparticles. *J. Am. Chem. Soc.* **2012**, *134*, 5722−5725.
(26) Yu, Z.; Pan, W.; Li, N.; Tang, B. A Nuclear Targeted Dual-Photosensitizer for Drug-Resistant Cancer Therapy with NIR Activated Multiple ROS. *Chem. Sci.* **2016**, *7*, 4237−4244.
(27) Hanson, L.; Zhao, W.; Lou, H.-Y.; Lin, Z. C.; Lee, S. W.; Chowdary, P.; Cui, Y.; Cui, B. Vertical Nanopillars for *In Situ* Probing of Nuclear Mechanics in Adherent Cells. *Nat. Nanotechnol.* **2015**, *10*, 554−562.
(28) Liu, X. J.; Ren, Q. L.; Fu, F. F.; Zou, R. J.; Wang, Q.; Xin, G. B.; Xiao, Z. Y.; Huang, X. J.; Liu, Q.; Hu, J. Q. CuS@mSiO$_2$-PEG Core-Shell Nanoparticles as a NIR Light Responsive Drug Delivery Nanoplatform for Efficient Chemo-Photothermal Therapy. *Dalton Trans.* **2015**, *44*, 10343−10351.
(29) Goel, S.; Chen, F.; Cai, W. B. Synthesis and Biomedical Applications of Copper Sulfide Nanoparticles: From Sensors to Theranostics. *Small* **2014**, *10*, 631−645.
(30) Li, N.; Yang, H. J.; Yu, Z. Z.; Li, Y. L.; Pan, W.; Wang, H. Y.; Tang, B. Nuclear-Targeted siRNA Delivery for Long-Term Gene Silencing. *Chem. Sci.* **2017**, *8*, 2816−282.
(31) Zhou, M.; Zhang, R.; Huang, M.; Lu, W.; Song, S.; Melancon, M. P.; Tian, M.; Liang, D.; Li, C. A Chelator-Free Multifunctional [Cu-64]CuS Nanoparticle Platform for Simultaneous Micro-PET/CT Imaging and Photothermal Ablation Therapy. *J. Am. Chem. Soc.* **2010**, *132*, 15351−15358.
(32) Chen, F.; Hong, H.; Goel, S.; Graves, S. A.; Orbay, H.; Ehlerding, E. B.; Shi, S.; Theuer, C. P.; Nickles, R. J.; Cai, W. *In Vivo* Tumor Vasculature Targeting of CuS@MSN Based Theranostic Nanomedicine. *ACS Nano* **2015**, *9*, 3926−3934.
(33) Tian, Q.; Hu, J.; Zhu, Y.; Zou, R.; Chen, Z.; Yang, S.; Li, R.; Su, Q.; Han, Y.; Liu, X. Sub-10 nm Fe_3O_4@$Cu_{2-x}S$ Core-Shell Nanoparticles for Dual-Modal Imaging and Photothermal Therapy. *J. Am. Chem. Soc.* **2013**, *135*, 8571−8577.
(34) Yu, Z.; Sun, Q.; Pan, W.; Li, N.; Tang, B. A Near-Infrared Triggered Nanophotosensitizer Inducing Domino Effect on Mitochondrial Reactive Oxygen Species Burst for Cancer Therapy. *ACS Nano* **2015**, *9*, 11064−11074.

DOI: 10.1021/acsnano.7b06870
ACS Nano 2018, 12, 5197−5206